

NASA TECHNICAL NOTE



NASA TN D-6012

e.1

LOAN COPY: RETURN TO:  
AWL (WLOL)  
KIRTLAND AFB, N ME



NASA TN D-6012

# APPLICATION OF A SUPERSONIC KERNEL-FUNCTION PROCEDURE TO FLUTTER ANALYSIS OF THIN LIFTING SURFACES

*by Herbert J. Cunningham*  
*Langley Research Center*  
*Hampton, Va. 23365*

# ERRATA

NASA Technical Note D-6012

## APPLICATION OF A SUPERSONIC KERNEL-FUNCTION PROCEDURE TO FLUTTER ANALYSIS OF THIN LIFTING SURFACES

By Herbert J. Cunningham

November 1970

In several places numerical values of generalized masses are given with units of slug-ft<sup>2</sup> and include conversion to units of kg-m<sup>2</sup>. The numerical values are correct, but the units should be slugs rather than slug-ft<sup>2</sup>. The converted numerical values are not correct for kg units. The following corrections should be made:

Page 13: The third sentence in the section "Model 1C" should be changed to read -

These masses in slugs (kg) were

$$\begin{bmatrix} m_{ij} \end{bmatrix} = 10^{-6} \begin{bmatrix} 58.0 & 90.8 & 71.9 \\ (846) & (1325) & (1049) \end{bmatrix}$$

Page 15: The sentence beginning on the third line below figure 4 should read -

The resulting masses in slugs (kg) are

$$\begin{bmatrix} m_{ij} \end{bmatrix} = 10^{-6} \begin{bmatrix} 55.6 & -8.95 & -2.68 \\ (811) & (-130.6) & (-39.1) \\ & 85.8 & -12.17 \\ & (1252) & (-177.6) \\ \text{Symmetric} & & 65.7 \\ & & (959) \end{bmatrix}$$

Page 31: Lines 8 and 9 in the section "Solution of the Flutter Determinant" should read -

$m_{11} = 0.0001905$  slug (0.002780 kg),  $m_{22} = 0.0003801$  slug (0.005547 kg),

$m_{33} = 0.0004918$  slug (0.007177 kg),  $m_{44} = 0.0001271$  slug (0.001855 kg),

Page 34: The second sentence of the second paragraph should be changed to read -

The numerical surface integrations produced the following matrix in units of slugs (kg) that can be compared with the values cited previously in the text:

$$\left[ n_{ij} \right] = 10^{-6} \begin{bmatrix} 182 & -0.4 & 17.2 & 8.6 \\ (2356) & (-6) & (251) & (126) \\ & 356 & -89.2 & -29.8 \\ & (5195) & (-1302) & (-435) \\ & & 472 & 41.0 \\ & & (6888) & (598) \\ \text{Symmetric} & & & 128 \\ & & & (1868) \end{bmatrix}$$

Page 38: Change the three generalized mass values in the table subheadings to -

$$m_{11} = 0.000357 \text{ slug (0.00521 kg)}$$

$$m_{22} = 0.000518 \text{ slug (0.00756 kg)}$$

$$m_{33} = 0.000264 \text{ slug (0.00385 kg)}$$

In addition, the following corrections should be made:

Page 5, line 1: The formula for air mass should be  $\left( \text{Air mass} = \rho \int_{y=0}^S \pi b^2 d(2b_0 y) \right)$

Page 18: Replace figure 7 with the attached figure. The error was in the ordinate scale for  $\frac{b_0 \omega_2}{a} \sqrt{\mu}$ .



0132780

1. Report No. <b>NASA TN D-6012</b>	2. Government Accession No.	3. Recipient's Catalog No.	
4. Title and Subtitle <b>APPLICATION OF A SUPERSONIC KERNEL-FUNCTION PROCEDURE TO FLUTTER ANALYSIS OF THIN LIFTING SURFACES</b>	5. Report Date <b>November 1970</b>		6. Performing Organization Code
	7. Author(s) <b>Herbert J. Cunningham</b>		8. Performing Organization Report No. <b>L-6808</b>
9. Performing Organization Name and Address <b>NASA Langley Research Center Hampton, Va. 23365</b>	10. Work Unit No. <b>126-14-14-01</b>		11. Contract or Grant No.
	12. Sponsoring Agency Name and Address <b>National Aeronautics and Space Administration Washington, D.C. 20546</b>		13. Type of Report and Period Covered <b>Technical Note</b>
15. Supplementary Notes		14. Sponsoring Agency Code	
16. Abstract  <p>A description is presented of a systematic procedure for obtaining generalized aerodynamic forces from the lifting-surface theory by the supersonic kernel-function method and for using those forces thus obtained in a Galerkin modal flutter analysis. The method is applicable to planforms with subsonic leading and supersonic trailing edges. Analytical flutter results were obtained and compared with experimental values from three flutter models.</p>			
17. Key Words (Suggested by Author(s)) <b>Lifting-surface flutter Aeroelasticity Dynamic loads</b>		18. Distribution Statement <b>Unclassified - Unlimited</b>	
19. Security Classif. (of this report) <b>Unclassified</b>	20. Security Classif. (of this page) <b>Unclassified</b>	21. No. of Pages <b>38</b>	22. Price <b>\$3.00</b>

# APPLICATION OF A SUPERSONIC KERNEL-FUNCTION PROCEDURE TO FLUTTER ANALYSIS OF THIN LIFTING SURFACES

By Herbert J. Cunningham  
Langley Research Center

## SUMMARY

Lifting-surface theory for supersonic flow, as analyzed by the supersonic kernel-function method, has been applied to obtain calculated flutter boundaries by a Galerkin modal flutter analysis. A systematic procedure for calculating the required generalized aerodynamic forces is described for a planform with subsonic leading and supersonic trailing edges. Analytical and experimental flutter characteristics are compared for three flutter-tested models. For two of the models, the analytical flutter speed ranges from slightly to moderately unconservative over a Mach number range of approximately 1.2 to 3.0. For the third model, the analytical flutter speed is slightly conservative. The agreement of analytical flutter frequencies with the experimental values is good for the three models.

## INTRODUCTION

An improved numerical procedure for calculating lifting pressures on harmonically deforming thin lifting surfaces by a supersonic kernel-function method, based on the linearized theory of unsteady potential flow, was described in reference 1. A lift-distribution series was developed for planforms with apex forward, subsonic leading edges, supersonic trailing edges, and (basically) pointed tips. The procedure was applied to the vibration modes of two root-cantilevered, platelike, low-aspect-ratio wings. For those wings, the desired or prescribed downwashes were compared graphically with the approximate downwashes that result from least-square-error solutions of the downwash equations. The agreement was good for the smoother downwashes; however, for the downwash distributions that fluctuated rather abruptly, particularly those for the real parts of the modes, the approximate downwashes did not follow the prescribed variations in detail.

The purpose of the present investigation is to further appraise the accuracy and adequacy of the lift-distribution series and its application in the kernel-function method by calculating flutter boundaries by a Galerkin modal method for comparison with some available experimental results from references 2 and 3 and from a model similar to those

described in reference 4. The computer program was extended, compatibly with the lift distribution series, to calculate generalized aerodynamic forces appropriate for the Galerkin formulation.

A description of the method of calculating the generalized aerodynamic forces is presented together with a comparison of analytical and experimental flutter boundaries. The flutter-equilibrium equations and the procedure for determining the analytical flutter characteristics and boundaries are described in appendix A. Appendix B gives an example of a computed flutter case.

Reference 5 is a recent report that treats essentially this same problem, that is, the lifting-surface integral equation that relates lift and downwash, which is applied to a planform with subsonic leading and supersonic trailing edges in supersonic flow and solved by a downwash collocation procedure. Unlike the present work, the first step in choosing a pressure series was to assume separation of the chordwise and spanwise variables. Also unlike the present work, the method of reference 5 applies to planforms with streamwise tips. A flutter calculation was made for comparison with one of the same experiments (from ref. 2) used in the present work.

#### SYMBOLS

$a$	speed of sound in test medium
$a_{n,m}^{(j)}$	weighting factors in the lift-distribution series for mode $j$ (see eq. (9))
$b$	local wing semichord
$b_0$	wing semichord at root or plane of symmetry
$b_{.75s}$	wing semichord at 0.75-semispan station ( $y = 0.75s$ )
$d_r$	coefficients in polynomials, where $r = 0, 1, 2, \dots$ (see eqs. (B1))
$G_1, G_2$	analytic integrals (see eqs. (15))
$g$	modal-independent damping coefficient in $g_i$
$g_i$	coefficient of structural, solid-friction damping for mode $i$ (see eqs. (A7) and (A10))
$g_{i,S}$	measured or assigned value of damping coefficient in $g_i$

$H(x,y,t)$	vertical displacement of lifting surface, positive with $z$
$h(\bar{x})$	chordwise distribution of mode-shape deflections approximated for numerical integration
$h_i, h_j$	amplitude of natural mode-shape deflection for modes $i$ and $j$ (see, for example, eq. (1))
$I_c(x_c), I_\sigma(y_\sigma)$	elements of integrating matrices for chordwise and spanwise integration, respectively (see eqs. (14) and (16))
$\text{Im}(\ )$	imaginary part of $(\ )$
III	transfer matrix (see eq. (10) and ref. 1)
$i$	unit of imaginaries, $\sqrt{-1}$
$k$	reduced frequency with reference length $b_0$ , $k \equiv \frac{\omega b_0}{V}$
$L_j(x,y)$	nondimensional lift distribution associated with mode $j$ (see eq. (8))
$l_n, l_n^*$	terms of lift-distribution series where $n = 0, 1, \dots, 5$ (see eqs. (9) and (10))
$M$	Mach number of stream flow, $V/a$
$m_A$	mass per unit area of lifting surface
$m_{ij}$	generalized mass (see eq. (A3))
$N$	number of modes in modal flutter analysis
$\Delta p$	lifting-pressure distribution, positive with $z$ (see eq. (4))
$\Delta p_j$	lifting-pressure distribution per unit $q_j/2b_0$ for mode $j$ (see eqs. (4) and (8))
$Q_i$	generalized aerodynamic-force quantity for mode $i$ (see eqs. (3) and (5))

$Q_{ij}, Q_{ij}^*$	dimensional and nondimensional generalized aerodynamic forces (see eqs. (5) and (11))
$q_j$	generalized coordinate of motion for mode $j$ , $\bar{q}_j e^{i\omega t}$
$\bar{q}_j$	complex amplitude of $q_j$
$\text{Re}(\ )$	real part of ( )
$s$	$y$ coordinate at right-hand wing tip
$t$	time
$V$	velocity of undisturbed air or other test medium
$w_j$	amplitude of downwash distribution per unit $q_j/2b_0$ at lifting surface for mode $j$ , positive with $z$ (see eqs. (6) and (7))
$X, Y, Z$	axis system of planforms
$x, y, z$	nondimensional chordwise, spanwise, and vertical coordinates, referred to $2b_0$
$x_c$	$x$ coordinate of points at which integrands are evaluated for numerical chordwise integration, where $c = 1, 2, \dots$
$\bar{x}$	nondimensional local section chordwise coordinate, referred to local chord (see eq. (B2))
$y_\sigma$	$y$ coordinate of span stations at which chordwise integrations are done for subsequent spanwise integration, where $\sigma = 1, 2, \dots$
$\alpha$	mass of air contained in the volume $4\pi b_0^3$ , $\alpha \equiv 4\pi\rho b_0^3$
$\Gamma_{ij}$	elements of flutter equilibrium equations and flutter determinant (see eqs. (A12) and (A13))
$\gamma_i$	quantity in flutter equation (A12)

$\mu$	ratio of mass of semispan wing to air mass $\left( \text{Air mass} = \rho \int_{y=0}^s \pi b^2 d(2b_0 y) \right)$
$\nu$	number of spanwise integration stations (odd in the present report)
$\rho$	density of air or other test medium
$\Omega$	complex frequency eigenvalue (see eq. (A12))
$\omega$	circular frequency of harmonic motion
$\omega_B$	chosen base or reference frequency
$\omega_i$	normal-mode natural frequency of mode $i$

Subscripts:

exp	experimental
i,j	mode numbers
le	value at wing leading edge
m	integers associated with exponent $m$ on $y^m$
n	integers associated with lift term $l_n$ or $l_n^*$
te	value at wing trailing edge
th	theoretical (analytical)
$\nu$	highest numbered (usually the most outboard) spanwise integration station

## ANALYSIS

### Origin of Analysis and Galerkin Modal Formulation

The present report is an outgrowth and extension of the work of reference 1. Its purpose is to describe a procedure for the calculation of generalized aerodynamic forces for a Galerkin modal formulation and to report the results of several flutter calculations made for comparison with experimental results. The planform treated is that shown in

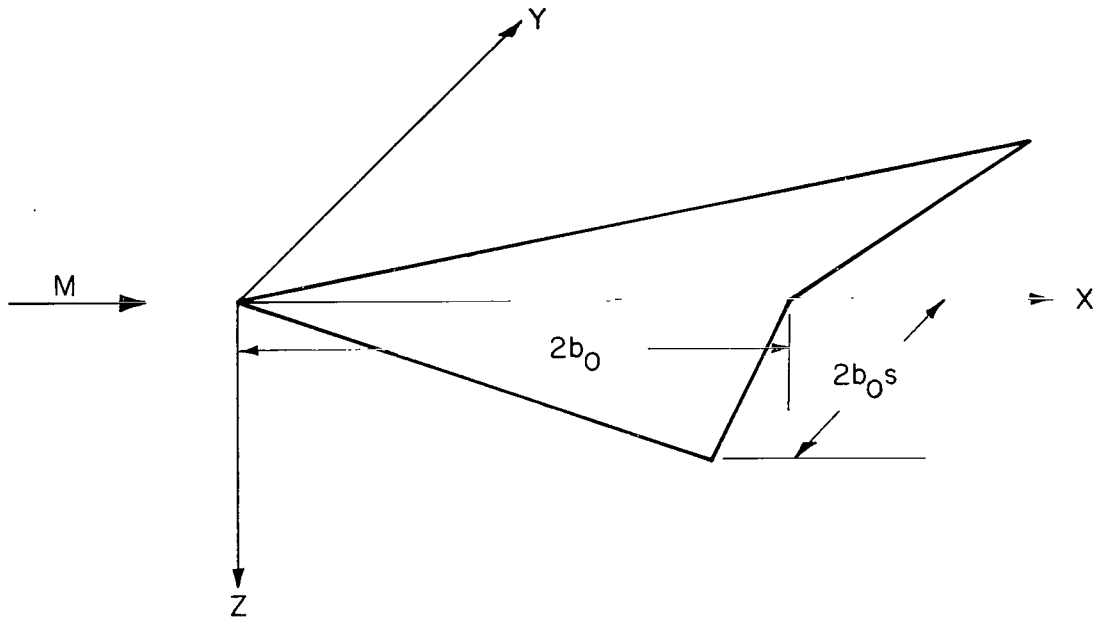


Figure 1.- Perspective view of lifting surface and coordinate system.

figure 1. The analysis applies for subsonic leading edges, supersonic trailing edges, and for (basically) pointed tips. The flutter-equilibrium equations are developed in appendix A, essentially in accord with existing practice, in order to make readily available the framework in which the aerodynamic forces are applied and from which flutter solutions are obtained.

In the Galerkin method, the location  $H(x,y,t)$  of the deformed or displaced surface is approximated by a finite series of chosen modes (see eq. (7) of ref. 1) that satisfy the boundary conditions of the structure:

$$H(x,y,t) \approx \sum_j h_j(x,y)q_j(t) \quad (1)$$

where for each mode  $j$ ,  $h_j(x,y)$  is the nondimensional mode shape,  $q_j(t)$  is the dimensional generalized coordinate of motion, and  $t$  is time.

The generalized aerodynamic forces required for flutter calculations arise from simple harmonic motion; that is,

$$q_j(t) = \bar{q}_j e^{i\omega t} \quad (2)$$

where  $\bar{q}_j$  is the complex amplitude of  $q_j$  and  $\omega$  is the circular frequency of harmonic motion.

## Generalized Aerodynamic Forces

In the Galerkin method, the generalized force  $Q_i$  is

$$Q_i = (2b_0)^2 \int_0^s \int_{x_{1e}}^{x_{te}} h_i \Delta p(x,y,t) dx dy \quad (3)$$

where  $h_i \equiv h_i(x,y)$  is defined in equation (1),  $x$  and  $y$  are nondimensional chordwise and spanwise coordinates, respectively,  $2b_0$  is the root chord length,  $s$  is the  $y$  coordinate of the wing tip,  $x_{1e}$  and  $x_{te}$  are the  $x$  coordinates of leading and trailing edges, respectively, and  $\Delta p(x,y,t)$  is the lifting-pressure distribution over the lifting surface that appears in the downwash integral equation, equation (1) of reference 1.

In keeping with the modal representation, the lifting pressure  $\Delta p$  is replaced by a modal series

$$\Delta p(x,y,t) = \sum_j \frac{q_j}{2b_0} \Delta p_j(x,y,t) \quad (4)$$

where  $\Delta p_j(x,y,t)$  is the lifting pressure that is associated with the deflection in mode  $j$  per unit value of  $q_j/2b_0$ .

The use of equation (4) in equation (3) leads to a modal series for  $Q_i$

$$Q_i = \sum_j q_j Q_{ij} \quad (5a)$$

where

$$Q_{ij} = 2b_0 \int_0^s \int_{x_{1e}}^{x_{te}} h_i \frac{\Delta p_j(x,y,t)}{e^{i\omega t}} dx dy \quad (5b)$$

The lifting pressure  $\Delta p_j$  is related to the motion in mode  $j$  in terms of its associated downwash  $w_j$  per unit  $q_j/2b_0$  by the downwash integral equation

$$-\frac{w_j(x,y,t)}{V} = \frac{(2b_0)^2}{4\pi\rho V} \int_{\eta_L}^{\eta_R} \int_{\xi_{1e}}^{\xi_{MC}} \Delta p_j(\xi,\eta,t) K(M,k,x-\xi,y-\eta) d\xi d\eta \quad (6)$$

where  $\xi$  and  $\eta$  are dummy variables for  $x$  and  $y$ , respectively, and  $K(M,k,x-\xi,y-\eta)$  is the supersonic kernel function in which  $M$  is Mach number and  $k = \frac{\omega b_0}{V}$  is the reduced frequency with reference length  $b_0$ . (The limits of integration  $\eta_R$ ,  $\eta_L$ ,  $\xi_{MC}$ , and  $\xi_{1e}$  are given in ref. 1.)

The downwash ratio for mode  $j$  is

$$\frac{w_j(x,y,t)}{V} = \left[ \frac{\partial h_j(x,y)}{\partial x} + i2kh_j(x,y) \right] e^{i\omega t} \quad (7)$$

The pressures  $\Delta p_j$  are expressed in terms of nondimensional quantities  $L_j(x,y)$  as in equation (12) of reference 1

$$\Delta p_j(x,y,t) = 4\pi \left( \frac{\rho V^2}{2} \right) L_j(x,y) e^{i\omega t} \quad (8)$$

In reference 1,  $L_j(x,y)$  is approximated by a linear combination of chosen functions of the form  $l_n(x,y)y^m$ , each with an initially undetermined complex weighting factor  $a_{n,m}^{(j)}$ , this relationship, given in matrix form, is

$$L_j(x,y) \approx \left[ l_n(x,y)y^m \right] \left\{ a_{n,m}^{(j)} \right\} \quad (9)$$

The 16 complex functions  $l_n y^m$  of reference 1 were chosen to provide good matrix conditioning in least-square-error solutions for the 16 weighting factors  $a_{n,m}^{(j)}$  from the set of equations for the downwash at selected downwash control points. But in order to improve computational efficiency at other stages of the overall calculation, the functions  $l_n y^m$  are expressed in terms of 46 real elements  $l_n^* y^m$  through a transformation matrix III as follows:

$$\left[ l_n y^m \right] = \left[ l_n^* y^m \right] \left[ \text{III} \right] \quad (10)$$

where the terms  $l_n^*$  and the matrix III are given by equation (13) and table I, respectively, of reference 1. (It should be noted that unlike the lift-distribution functions that are used frequently in the subsonic kernel-function methods, the elemental functions  $l_n^*(x,y)$  in the present supersonic kernel approach do not feature separation of the chordwise and spanwise variables  $x$  and  $y$ .)

Substitution of equations (8), (9), and (10) into equations (5) gives

$$Q_{ij} = 4\pi\rho V^2 b_0 Q_{ij}^* \quad (11a)$$

where

$$Q_{ij}^* = \int_0^S dy \int_{x_{1e}}^{x_{te}} h_i \left[ l_n^* y^m \right] \left[ \text{III} \right] \left\{ a_{n,m}^{(j)} \right\} dx \quad (11b)$$

and  $Q_{ij}^*$  are the nondimensional generalized aerodynamic-force elements. The surface integration indicated in equations (11) is carried out by numerical quadrature, first chordwise and then spanwise. The procedure that is the most economical of computing time

is integration of the product of  $h_i$  and each of the 46 elements in  $[l_n^* y^m]$  followed by postmultiplication of the resulting row of 46 integrals by  $[III] \{a_{n,m}^{(j)}\}$ .

Chordwise integration.- The chordwise integrals are obtained at the span stations required by the spanwise integration. Two of the lift-distribution terms  $l_0^*$  and  $l_1^*$  have integrable singularities at the wing leading edge. Consequently, the accuracy of the chordwise integration is improved if  $h_i(x,y)$  is replaced by its identity

$$h_i(x,y) \equiv [h_i(x,y) - h_i(x_{1e},y)] + h_i(x_{1e},y) \quad (12)$$

so that the chordwise integral for any term  $l_n^*$  becomes

$$\int_{x_{1e}}^{x_{te}} h_i(x,y) l_n^*(x,y) dx = \int_{x_{1e}}^{x_{te}} [h_i(x,y) - h_i(x_{1e},y)] l_n^*(x,y) dx + h_i(x_{1e},y) \int_{x_{1e}}^{x_{te}} l_n^*(x,y) dx \quad (13)$$

The integrand of the first integral is zero at the leading edge, and integration of the second integral can be performed analytically with high accuracy.

For any span station, the chordwise integrations of the array of terms  $l_n^*$  are indicated in the following matrix operation:

$$\begin{aligned} & \begin{matrix} n \downarrow \\ \left[ \begin{matrix} l_n^*(x_c, y_\sigma) \end{matrix} \right] \\ \text{matrix (1)} \end{matrix} \begin{matrix} c \leftarrow \\ \left[ \begin{matrix} I_c(x_c) \end{matrix} \right] \\ \text{matrix (2)} \end{matrix} \begin{matrix} i \rightarrow \\ \left[ \begin{matrix} h_i(x_c, y_\sigma) \\ - h_i(x_{1e}, y_\sigma) \end{matrix} \right] \\ \text{matrix (3)} \end{matrix} \\ & + \begin{matrix} n \downarrow \\ \left[ \begin{matrix} h_i(x_{1e}, y_\sigma) \int_{x_{1e}}^{x_{te}} l_n^*(x, y_\sigma) dx \end{matrix} \right] \\ \text{matrix (4)} \end{matrix} = \begin{matrix} n \downarrow \\ \left[ \begin{matrix} \text{Chordwise integrals of} \\ h_i l_n^* \text{ as in eq. (13)} \end{matrix} \right] \\ \text{matrix (5)} \end{matrix} \quad (14) \end{aligned}$$

where  $x_c$  and  $y_\sigma$  are the  $x$  and  $y$  coordinates, respectively, of the array of points along the chord at which integrand quantities are evaluated for span station  $y_\sigma$ . The order and dimension of each matrix are indicated with arrows as follows:  $n \downarrow$  means  $n$  varies from 0 in the first row to 5 in the sixth row;  $c \leftarrow$  (or  $c \downarrow$ ) indicates as many columns (or rows) as there are points  $x_c$  along the chord; and  $i \rightarrow$  means that mode  $i$  ranges from 1 to  $N$ , the number of modes in the analysis. Each matrix has a designation for convenience of referral. The elements  $I_c(x_c)$  in the diagonal matrix, matrix (2), are the integrating factors for chordwise integration.

The values of the chordwise integrals in the elements of matrix (4) of equation (14) are found from their analytical expressions that are tabulated as follows for any span station  $y_\sigma$ :

n	Integral, $\int_{x_{1e}}^{x_{te}} l_n^*(x, y_\sigma) dx$
0 . . . . .	$G_1$
1 . . . . .	$\frac{G_1 x_{te} + G_2}{2}$
2 . . . . .	$\frac{G_1 x_{te} - G_2}{2}$
3 . . . . .	$\frac{G_1^3}{3}$
4 . . . . .	$\frac{2G_1^3 x_{te} + G_1 x_{1e}^2 x_{te} - G_2 x_{1e}^2}{8}$
5 . . . . .	$\frac{G_1^5}{5} + \frac{G_1^3 x_{1e}^2}{3}$

where

$$\left. \begin{aligned} G_1 &= \sqrt{x_{te}^2 - x_{1e}^2} \\ G_2 &= x_{1e}^2 \cosh^{-1} \left| \frac{x_{te}}{x_{1e}} \right| \end{aligned} \right\} \quad (15)$$

The numerical integration that is accomplished by the first matrix product in equation (14) (matrix (1)  $\times$  matrix (2)  $\times$  matrix (3)) can be performed by any suitable rule. In the present work, Gaussian quadrature was used because of its known accuracy. The choice of rule determines the locations  $x_c$  and the associated integrating factor  $I_c(x_c)$ . The computing program permits other types of numerical quadrature at the option of the user, who must then supply "nonstandard" input data for the arrays of  $x_c$  and  $I_c(x_c)$ . Often the deflections  $h_i(x_c, y_\sigma)$  are not known at the points  $x_c$ , and interpolation is necessary.

Spanwise integration.- When the matrix operation of equation (14) is carried out for the span stations  $y_\sigma$  in sequence, matrix (5) takes on a third dimension equal to the number of span stations. The spanwise integration is indicated by the following matrix operation:



reference 1 is produced to keep the operation simpler to this point. But for each mode  $i$ , 14 elements are discarded, the remaining 46 elements are rearranged, and the matrix of  $Q_{ij}^*$  is computed as follows:

$$\begin{array}{ccccccc}
 46 \text{ columns} \rightarrow & 16 \text{ columns} \rightarrow & & j \rightarrow & & j \rightarrow & \\
 i \downarrow & \left[ \begin{array}{c} \text{Surface} \\ \text{integrals} \end{array} \right] & \begin{array}{c} 46 \\ \text{rows} \\ \downarrow \end{array} & \left[ \text{III} \right] & \begin{array}{c} 16 \\ \text{rows} \\ \downarrow \end{array} & \left[ \begin{array}{c} a_{n,m}^{(j)} \end{array} \right] & = & i \downarrow \left[ \begin{array}{c} Q_{ij}^* \end{array} \right] \\
 & \text{matrix (8x)} & & & & & & (18)
 \end{array}$$

Each row of the rearranged matrix (8x) is for one of the modes and is obtained from the elements of matrix (8) for that mode by using the following elements: all 10 elements from the first row of matrix (8), the first eight elements from row two, all 10 elements from row three, the first eight elements from row four, the first six elements from row five, and the first four elements from row six – a total of 46 elements. The elements of  $\left[ \text{III} \right]$ ,  $\left[ a_{n,m}^{(j)} \right]$ , and  $\left[ Q_{ij}^* \right]$  are complex quantities, in general. Matrices (1) to (8x) all have real-number elements.

## RESULTS AND DISCUSSION

The present procedure for calculating generalized aerodynamic forces has been applied in a Galerkin modal analysis, described in appendix A, to determine the flutter characteristics and boundaries of three different flutter-test models for which experimental results were available. These models include the semispan, root cantilevered, flat-plate flutter models of reference 2, that is, model 1A with a  $70^\circ$  swept delta planform and model 1C with an  $80^\circ$  swept delta planform. The third is a flutter model designated HT-7 that was a variation of the HT series of reference 4, but which was tested subsequent to the preparation of reference 4.

### Model 1A

The planform of model 1A is shown in figure 2.

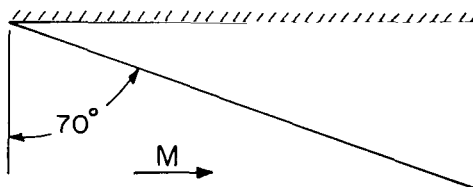


Figure 2.- Planform of model 1A.

A comparison of complex downwash results for this model was presented in figure 5 of reference 1 for the first two vibration modes for  $M = 2.0$  and  $k = 0.5$ . For the present analysis, all four modes of table II(a) of reference 2 were used. Appendix B includes a description of how the general mode shape and downwash information was interpolated from the limited data of that table. Forty-eight downwash control points were used, as described in appendix B, rather than the 46 that gave the results in reference 1.

Figure 3 and table I present the stiffness-altitude parameter  $\frac{b \cdot 75s \omega^2}{a} \sqrt{\mu}$  and the ratio of analytical to experimental flutter frequency as functions of Mach number. The results of the present kernel-function analysis are plotted for each experimental supersonic Mach number, beginning with  $M = 1.19$ , except at the upper limit for a subsonic leading edge,  $M = 2.92$ , the analytical point was calculated by using the wing parameters for the experiment at  $M = 3.0$ . The experimental and piston-theory results from reference 2 are repeated on the figures for comparison. The kernel-function results for stiffness-altitude parameter fall mostly between the piston-theory results and the experiment (except for  $M = 1.19$ ), and thus are still slightly to moderately unconservative in comparison with the experiment. (By unconservative, it is meant that the stiffness required to prevent flutter determined analytically was found to be less than that determined experimentally.) The calculation for  $M = 2.0$  is described in appendix B. The values for the analytical flutter frequency are within 6 percent of the experimental value for five of the six cases presented and within 11 percent for the other case.

Reference 5 reports the results of a flutter calculation for this same model 1A for  $M = 2.0$ . That calculation used a different pressure-mode series, a different collocation, and analytically rather than experimentally determined mode shapes and frequencies. The calculated stiffness-altitude parameter was unconservative by only about 5 percent in comparison with experimental value and the flutter frequency was within 1 percent of the experimental value.

### Model 1C

The planform of model 1C is shown in figure 4. For this model, calculations were first made with three modes and with the diagonal generalized mass matrix that was used in obtaining the piston-theory results in reference 2. These masses in  $\frac{\text{slug} \cdot \text{ft}^2}{\text{slug}} (\text{kg} \cdot \text{m}^2)$  were

$$[m_{ij}] = 10^{-6} \begin{bmatrix} 58.0 & 90.8 & 71.9 \\ \cancel{(78.6)} & \cancel{(123.1)} & \cancel{(97.5)} \\ (846) & (1325) & (1049) \end{bmatrix}$$

The resulting flutter boundary, in terms of the stiffness-altitude parameter, was widely unconservative; and the flutter frequency was near the third-mode frequency rather than being below the second-mode frequency as the experimental value was. The root that

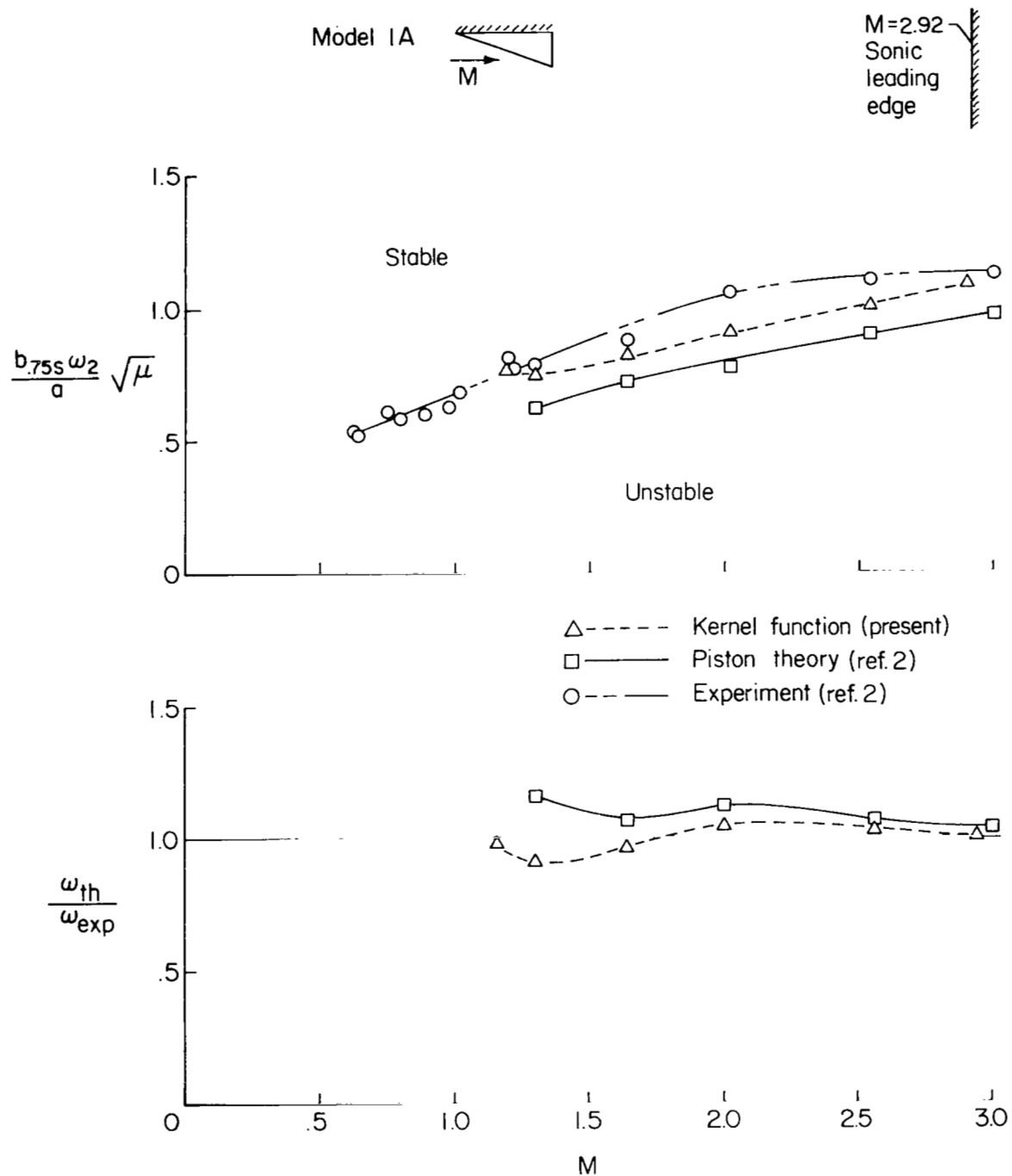


Figure 3.- Flutter boundary in terms of stiffness-altitude parameter and ratio of analytical to experimental flutter frequency as a function of Mach number for model IA.

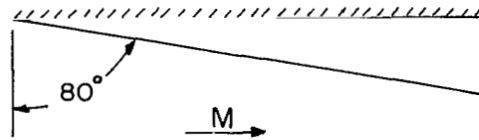


Figure 4.- Planform of model 1C.

originated from mode 3 is the one that became unstable. In view of the serious lack of agreement between analysis and experiment, it was decided to calculate new generalized masses on the basis of the interpolations from equation (B3). The resulting masses in ~~slug-ft<sup>2</sup> (kg-m<sup>2</sup>)~~ are  
slugs (kg)

$$[m_{ij}] = 10^{-6} \begin{bmatrix} 55.6 & -8.95 & -2.68 \\ \cancel{(75.4)} & \cancel{(-12.13)} & \cancel{(-3.03)} \\ (811) & (-130.6) & (-39.1) \\ & 85.8 & -12.17 \\ & \cancel{(116.3)} & \cancel{(-17.2)} \\ & (1252) & (-177.6) \\ & & 65.7 \\ \text{Symmetric} & & \cancel{(80.02)} \\ & & (959) \end{bmatrix}$$

and their use along with the modal frequencies of model 1C produced the results listed in table I and plotted in figure 5. Even though the off-diagonal, mass-coupling elements are small compared with the on-diagonal direct elements, their effect is decisive in determining the flutter characteristics since they cause the mode 2 root, rather than the mode 3 root, to become unstable. This difference caused a great improvement in the calculated frequency (three out of five frequencies within 5 percent of the experimental values and another within 10 percent) and a substantial improvement in the stiffness-altitude parameter, although the latter is still somewhat unconservative, as it was for model 1A. The same comments as for model 1A apply concerning the unconservativeness. A comparison of tables I and II(c) of reference 2 discloses that the frequencies for the "representative mode shapes" in table II(c) are noticeably higher than those given in table I therein for the models actually fluttered. Whether this higher frequency has any significant effect on the mode shapes is only conjectural. (Incidentally, in table I of reference 2 there are two incorrect numbers at  $M = 2.0$  for model 1C. The cyclic frequency  $f_2$  should be 367 Hz rather than 467 Hz, and density  $\rho$  should be 0.001418 slug/ft<sup>3</sup> (0.731 kg/m<sup>3</sup>) rather than 0.001468 slug/ft<sup>3</sup> (0.7566 kg/m<sup>3</sup>.)

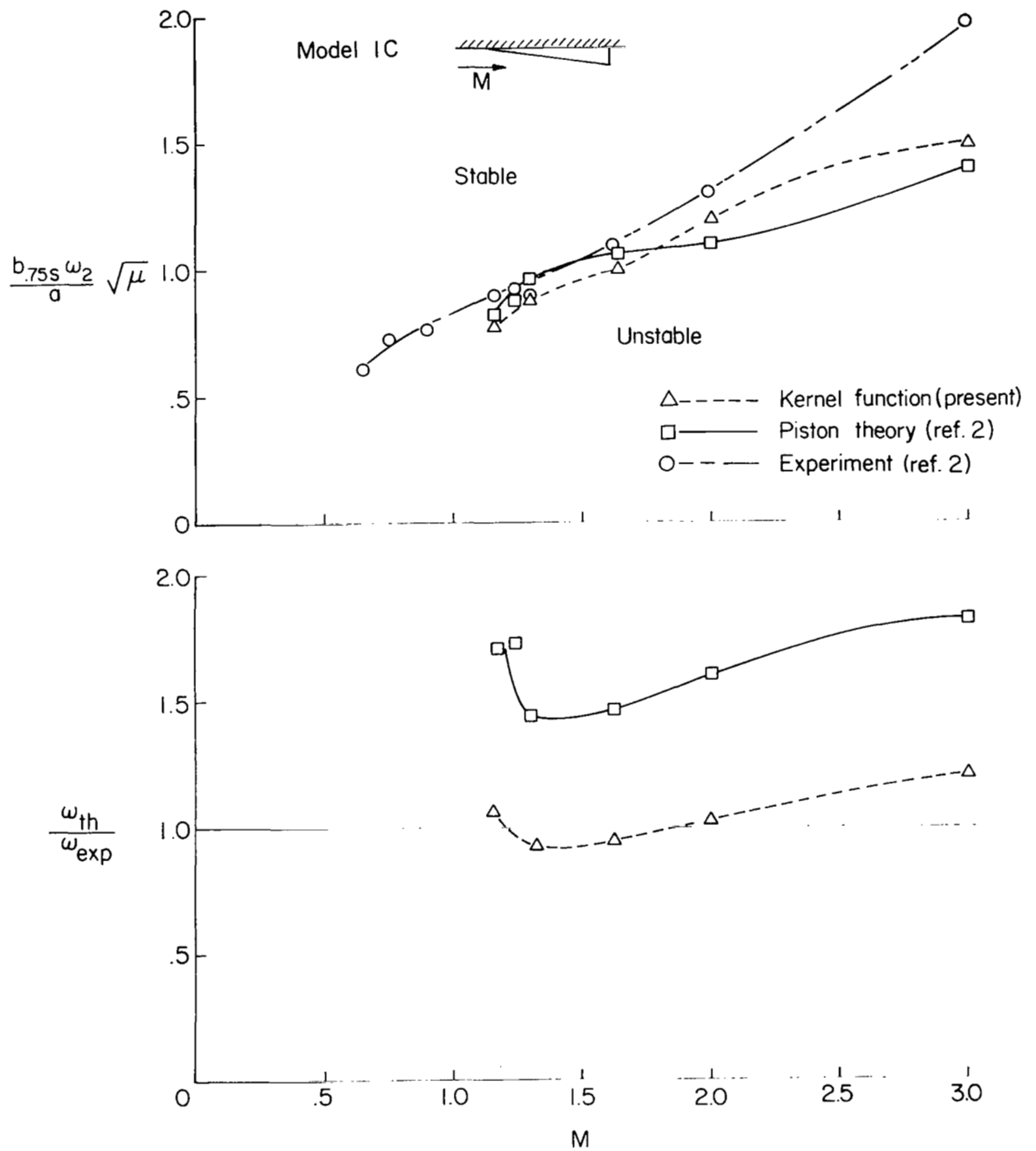


Figure 5.- Flutter boundary in terms of stiffness-altitude parameter and ratio of analytical to experimental flutter frequency as a function of Mach number for model IC.

## Model HT-7

The planform of model HT-7 is shown in figure 6.

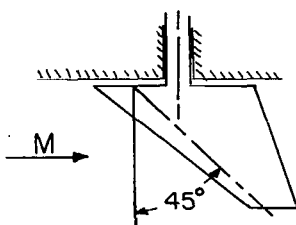


Figure 6.- Planform of model HT-7.

In seeking additional flutter experiments to which the present analysis could be compared, reference 4 was considered. There, the all-movable horizontal-tail models are of primary interest because, in spite of the cut-off tip, the relative proportion of the surface area that is affected by the cut-off tips is small and because the models had neither control surfaces nor leading-edge breaks to complicate the analysis. Unfortunately, there is not sufficient information in reference 4 on mode shapes of the HT (horizontal tail) series. Unpublished data were found, however, on a variation (HT-7) of the HT series that was successfully flutter tested. The available modal data are listed herein in table II. The parameters for the flutter experiment were as follows:  $M = 1.64$ ,  $V = 1300$  ft/sec (396.2 m/sec),  $\rho = 0.003305$  slug/ft<sup>3</sup> (1.703 kg/m<sup>3</sup>), Dynamic pressure = 2790 lb/ft<sup>2</sup> (133.59 kN/m<sup>2</sup>),  $\omega/\omega_2 = 0.683$ , and  $V/b_0\omega_2 = 2.09$ .

For this surface, the aspect ratio is 2.50, the taper ratio is 0.3, the sweepback angles are 50.5° for the leading edge and 45° for the quarter-chord line, and the Mach number for a sonic leading edge is 1.573, which is the upper limit of the subsonic leading-edge range in which calculations can be made by the present analysis. Calculations were made for  $M = 1.2, 1.3, 1.4,$  and  $1.573$  by using the experimental density  $\rho = 0.003305$  slug/ft<sup>3</sup> (1.703 kg/m<sup>3</sup>). Figure 7 includes curves faired through the point values obtained for  $\frac{b_0\omega_2}{a}\sqrt{\mu}$  and  $\omega/\omega_2$ . The experimental values are plotted at  $M = 1.64$ , and the results obtained from aerodynamic piston theory are obtained from figure 10 of reference 3 for comparison. A smooth extrapolation of the analytical results to the Mach number of the experiment yields good agreement for the frequency and a small conservative margin for the stiffness-altitude parameter.

Based on the analyses and the comparisons with experiment that have been presented, the application of the lifting-pressure series of reference 1 in the present procedure for calculating flutter characteristics is concluded to be rather accurate and adequate overall and, therefore, to have useful areas of application.

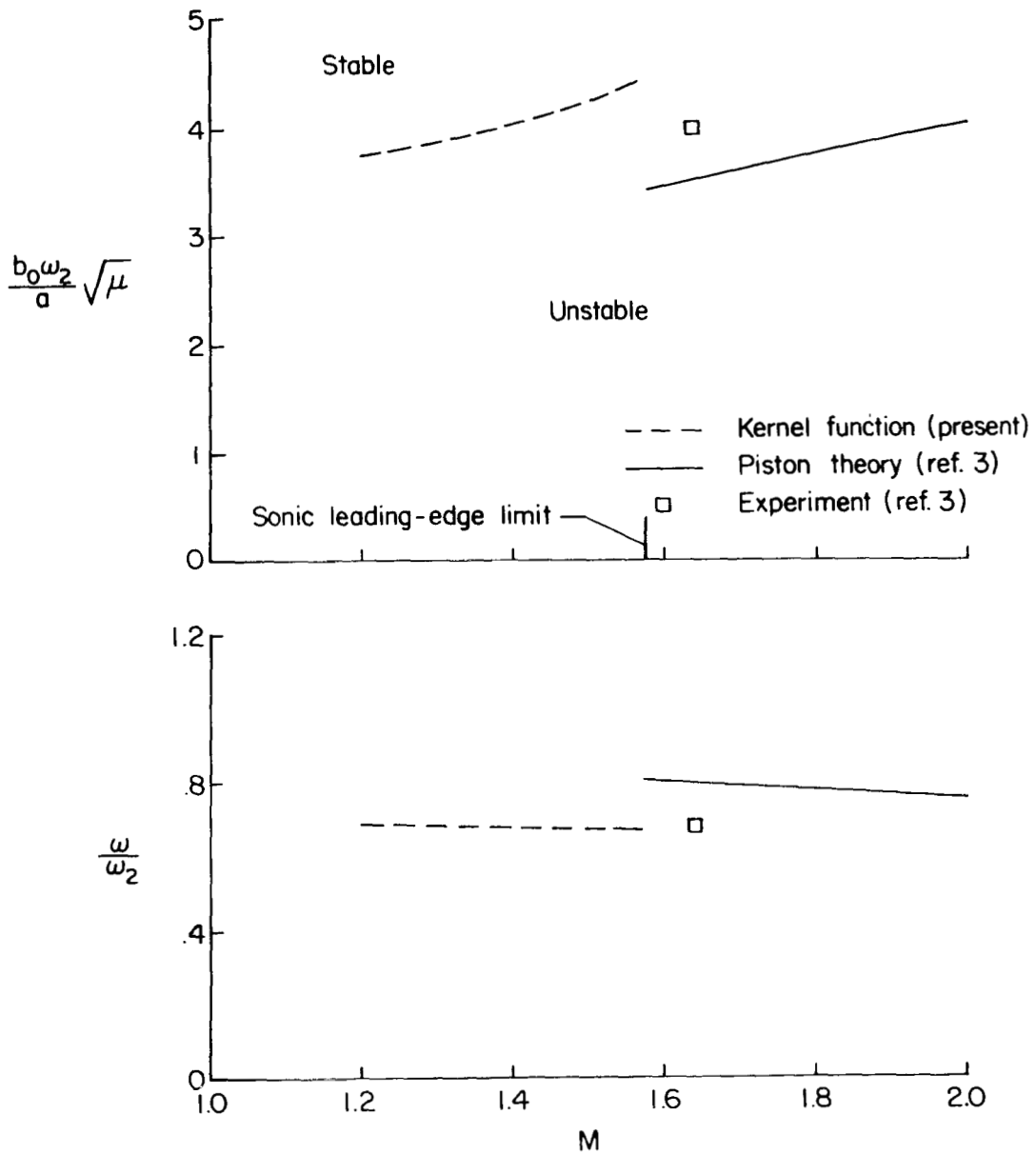


Figure 7.- Flutter boundary in terms of the stiffness-altitude parameter and ratio of flutter frequency to second natural frequency as a function of Mach number for an all-movable control-surface model, HF-7.

## CONCLUDING REMARKS

A description is presented of a systematic procedure for obtaining generalized aerodynamic forces from the lifting-surface theory by the supersonic kernel-function method and for using those forces obtained in a Galerkin modal flutter analysis. Analytical flutter results are presented for three different flutter models and compared with their experimental results.

For two of the models the analytical flutter results in terms of stiffness-altitude parameter are slightly to moderately unconservative in comparison with the experimental results, and the flutter-frequency agreement is within 6 percent for eight of 11 cases and within 11 percent for two of the other three cases. For the third model, analytical results were obtained over a Mach number range up to 1.573 for which the leading edges are subsonic. A smooth extrapolation of the results to the Mach number of the experiment, 1.64, yielded good agreement with experimental results for the frequency and a small conservative margin for the stiffness-altitude parameter. The procedure presented herein, therefore, appears to have useful areas of application.

Langley Research Center,  
National Aeronautics and Space Administration,  
Hampton, Va., August 19, 1970.

## APPENDIX A

### FLUTTER EQUATIONS FROM A GALERKIN FORMULATION AND SOLUTIONS FOR FLUTTER CHARACTERISTICS

Flutter characteristics and boundaries are determined from the equations of equilibrium for the structure. Here, those equations of equilibrium are formulated based on the Galerkin modal approach, beginning from the fundamentals essentially as described in reference 6.

#### Mathematical Model

The lifting surface is considered nearly planar with a mean location nearly in the XY-plane as shown in figure 1. A small displacement or deformation  $H(x,y,t)$  of the surface away from its mean location during flutter is approximated by a finite series, as indicated in equation (1) (see also eq. (7) of ref. 1). This equation is repeated here for convenience:

$$H(x,y,t) \approx \sum_j h_j(x,y)q_j(t) \quad (A1)$$

where for each mode  $j$ ,  $h_j(x,y)$  is the nondimensional mode-shape distribution and  $q_j(t)$  is the generalized coordinate of motion. The start of flutter (neutral-stability condition) is defined by the existence of simple harmonic motion so that  $q_j(t) = \bar{q}_j e^{i\omega t}$ .

#### Equations of Equilibrium

With the modal representation of equation (A1), the Galerkin procedure results in the following equations for no internal damping:

$$q_i \omega_i^2 m_{ii} - \sum_j q_j \omega_j^2 m_{ij} - Q_i = 0 \quad (i = 1, 2, \dots) \quad (A2)$$

where the generalized masses are

$$m_{ij} = (2b_0)^2 \int_0^S \int_{x_{1e}}^{x_{te}} m_A h_i h_j dx dy \quad (A3)$$

the generalized aerodynamic force quantity, given as equation (3) previously, is

$$Q_i = (2b_0)^2 \int_0^S \int_{x_{1e}}^{x_{te}} h_i \Delta p(x,y,t) dx dy \quad (A4)$$

APPENDIX A - Continued

and  $\omega_i$  is the normal-mode natural frequency of mode  $i$ ,  $2b_0$  is the root chord length,  $m_A$  is the mass per unit area,  $s$  is the  $y$  coordinate of the right-hand wing tip,  $x_{le}$  and  $x_{te}$  are the  $x$  coordinates of the leading and trailing edges, respectively, and  $\Delta p(x,y,t)$  is the lifting-pressure distribution over the lifting surface.

The first term on the left-hand side of equation (A2) is the generalized stiffness represented in terms of  $\omega_i$  and  $m_{ii}$ , according to Rayleigh's principle. This term reflects the usual assumption that stiffness coupling between modes is negligible. The second term contains the generalized masses  $m_{ij}$  and allows the possibility of mass coupling between modes. The third term is the generalized aerodynamic force, which represents the work done on mode  $i$  by the aerodynamic forces from the overall motion.

The lifting-pressure distribution  $\Delta p$  in equation (A4) is expressed in terms of the contributions from the modes  $j$  of equation (A1) as

$$\Delta p(x,y,t) \approx \sum_j \frac{q_j}{2b_0} \Delta p_j(x,y,t) \quad (A5)$$

where  $\Delta p_j$  is the lifting-pressure distribution per unit value of  $q_j/2b_0$ . Application of equation (A5) to equation (A4) permits  $Q_i$  to be separated into a modal series, presented previously as equations (5a) and (11a), respectively,

$$Q_i = \sum_j q_j Q_{ij} \quad (A6a)$$

$$Q_{ij} = 4\pi\rho V^2 b_0 Q_{ij}^* \quad (A6b)$$

and the nondimensional generalized aerodynamic-force terms  $Q_{ij}^*$  are developed in the main text (see eq. (11b)).

Structural damping.- Provisions for structural damping are introduced in the customary way by multiplying the generalized stiffness term, the first term in equation (A2), by  $(1 + ig_i)$ , where  $g_i$  is the coefficient of structural, solid-friction damping for mode  $i$ . (The unit of imaginaries  $i \equiv \sqrt{-1}$  is not to be confused with the modal subscript  $i = 1, 2, \dots$ .) This type of structural damping is characterized by: (1) a resisting force that is in phase with velocity and proportional to amplitude and (2) mechanical energy dissipated per cycle of vibration, which is proportional to the square of the amplitude but independent of frequency.

Flutter equations.- Insertion of the damping term  $(1 + ig_i)$  in the first term of equation (A2) and substitution of equation (A6) in the same equation leads to the following form:

APPENDIX A - Continued

$$q_i \omega_i^2 (1 + ig_i) m_{ii} - \sum_j q_j (\omega^2 m_{ij} + 4\pi\rho V^2 b_0 Q_{ij}^*) = 0 \quad (i = 1, 2, \dots) \quad (A7)$$

The set of equations of dynamic equilibrium represented by equation (A7) contains two unknowns  $\omega$  and  $V$ . The aerodynamic force quantities  $Q_{ij}^*$  are complex functions of the reduced frequency  $k = \frac{\omega b_0}{V}$  that combines  $\omega$  and  $V$ . Therefore,  $\omega$  and  $V$  cannot be solved explicitly, and some procedure for searching for solution values is required. A commonly used method is to group terms dependent on  $k$  separately from those containing  $\omega$  only. This grouping is done by dividing equation (A7) by  $\omega^2$  and using the relations among  $\omega$ ,  $V$ , and  $k$  so that

$$q_i \left(\frac{\omega_i}{\omega}\right)^2 (1 + ig_i) m_{ii} - \sum_j q_j \left(m_{ij} + 4\pi\rho b_0^3 \frac{Q_{ij}^*}{k^2}\right) = 0 \quad (i = 1, 2, \dots) \quad (A8)$$

At this point, it can be seen that, for chosen combinations of  $\rho$  and  $k$ , eigensolutions can be made for  $(1/\omega^2)$ . In general  $1/\omega^2$  will be a complex quantity; if the real part is positive, the sign of the imaginary part is a qualitative indication of a damped (stable) or growing (unstable) oscillation. Points on flutter boundaries are obtained from combinations of  $\rho$  and  $k$  that result in zero imaginary parts for  $1/\omega^2$ , that correspond to neutrally stable, simple harmonic motion for which the aerodynamic forces are valid.

Equations (A8) are not, however, in a form ready for eigensolution by an eigenvalue subroutine. To put them in such a form, they are first multiplied by  $-\frac{(\omega_B/\omega_i)^2}{m_{ii}}$  to obtain

$$q_i \left[ -\left(\frac{\omega_B}{\omega}\right)^2 (1 + ig_i) \right] + \sum_j q_j \left[ \frac{m_{ij}}{m_{ii}} \left(\frac{\omega_B}{\omega_i}\right)^2 + \frac{4\pi\rho b_0^3}{m_{ii}} \left(\frac{\omega_B}{\omega_i}\right)^2 \frac{Q_{ij}^*}{k^2} \right] = 0 \quad (i = 1, 2, \dots) \quad (A9)$$

where  $\omega_B$  is a chosen "base" or reference frequency. In order to facilitate the search in the customary way for eigenvalues of  $(\omega_B/\omega)^2$  that are real only, and at the same time to retain the use of actual or assumed structural damping coefficients  $g_i$  that are different for different modes  $i$ , the asymptotic approximation introduced in reference 7 is adopted; that is,  $g_i$  is considered to be made up of two parts

$$g_i = g_{i,S} + g \quad (A10)$$

where  $g_{i,S}$  is the measured or assigned structural value for mode  $i$ , and  $g$  is a modal-independent increment that has the same interpretations as in past usage; that is, points on a flutter boundary are sought for which  $g = 0$ , and where  $g \neq 0$  that value of  $g$  is the amount that would have to be added to the structure to permit neutrally stable, simple harmonic motion. By using equation (A10)

APPENDIX A - Continued

$$1 + ig_i = 1 + ig_{i,S} + ig \sim (1 + ig_{i,S})(1 + ig) \quad (\text{A11})$$

where the asymptotic approximation appears on the right-hand side of the equation. Substituting equation (A11) into equation (A9) and dividing by  $1 + ig_{i,S}$  result in the following form that is ready for solution by a complex eigenvalue subroutine:

$$-\Omega q_i + \sum_j \Gamma_{ij} q_j = 0 \quad (i = 1, 2, \dots) \quad (\text{A12})$$

where

$$\Omega = \left( \frac{\omega_B}{\omega} \right)^2 (1 + ig)$$

$$\Gamma_{ij} = \gamma_i \left( m_{ij} + \alpha \frac{Q_{ij}^*}{k^2} \right)$$

$$\gamma_i = \frac{(\omega_B/\omega_i)^2}{m_{ii}(1 + ig_{i,S})}$$

$$\alpha = 4\pi\rho b_0^3$$

Nontrivial solutions (that is, all  $q_j \neq 0$ ) of the set of equations (A12) are obtained by setting the determinant of the matrix of the coefficients of the  $q_j$ 's equal to zero, giving the usual flutter determinant

$$\begin{vmatrix} -\Omega + \Gamma_{11} & \Gamma_{12} & \dots & \Gamma_{1N} \\ \Gamma_{21} & -\Omega + \Gamma_{22} & \dots & \Gamma_{2N} \\ \vdots & \vdots & \ddots & \vdots \\ \Gamma_{N1} & \Gamma_{N2} & \dots & -\Omega + \Gamma_{NN} \end{vmatrix} = 0 \quad (\text{A13})$$

where  $N$  represents the number of modes used. The eigenvalues  $\Omega$  of the flutter determinant can be found by any method that is applicable to complex non-Hermitian matrices. The subroutine used herein is based on that described in reference 8. Chosen combinations of  $\rho$  and  $k$  give, in general, complex values of  $\Omega$ . The positive real part  $(\omega_B/\omega)^2$  gives the frequency, and the ratio of imaginary part to real part gives the associated  $g$ . Thus, finding points on a flutter boundary means selecting combinations of  $\rho$  and  $k$  that result in  $g = 0$ .

## APPENDIX A - Continued

### Solutions for Flutter Boundaries

In preparation for a flutter-boundary solution, all the input quantities that characterize the structure and the flow are computed or are chosen according to the judgment of the analyst. These include structural information in terms of mode shapes, frequencies, generalized masses, structural damping coefficients, and locations of control points at which the downwash ratios for all modes  $j$  are obtained as

$$\frac{w_j(x,y,t)}{v} = \left( \frac{\partial}{\partial x} + i2k \right) h_j(x,y) q_j \quad (A14)$$

A staggered arrangement of control points is recommended as an aid in minimizing unwanted variations in downwash distributions between control points. (See appendix B.) Since separation of the chordwise and spanwise variables was not assumed in the pressure distributions  $l_n^*$ , none of the published schemes for optimizing the location of control points are applicable. Often mode shapes  $h_j$  from tests are not measured at the locations of the selected control points, and it becomes necessary to interpolate to get the desired downwash ratios.

Flow parameters that are to be selected include the Mach number, reduced frequency, and air density. The range and sequence in which the parameters are chosen depend upon the conditions for which flutter characteristics or flutter boundaries are to be calculated. These include: (a) calculation within a designated range of altitude and Mach number in the standard atmosphere; (b) more general calculations of variations among certain parameters, such as among Mach number, mass ratio, and flutter-speed index; and (c) calculations to be compared with known wind-tunnel results, as in the present work. For condition (c), the experimental Mach number is used together with an initial value of  $k$  estimated from

$$k = \frac{b_0 \omega_{\text{exp}}}{aM} \quad (A15)$$

where  $\omega_{\text{exp}}$  is the experimental flutter frequency and  $a$  is the speed of sound in the test medium. For this  $k$ , the nondimensional generalized aerodynamic forces  $Q_{ij}^*$  are calculated. A flutter determinant is formed for each of a range of values of  $\rho$  beginning well below the experimental value. For each  $\rho$ , the set of eigenvalues  $\Omega$  is calculated. The values of  $g$  are the ratios of  $\text{Im}(\Omega)/\text{Re}(\Omega)$  and for sufficiently low  $\rho$  are usually all negative (with positive  $\text{Re}(\Omega)$ ); this condition indicates stability. A progressive increase in  $\rho$  usually results in one or more of the modes (roots) becoming unstable; that is,  $g$  passes from negative, through zero, to positive. A sufficient range of  $\rho$  must be used to assure that the critical instability point, which is that point which requires the greatest stiffness to prevent flutter, is found. If the flutter point thus found does not occur at the density of interest or if results are desired over a range of density, the

APPENDIX A - Continued

calculations are repeated for other values of  $k$ . In selecting other values of  $k$ , some guidance can be obtained from the fact that for a fixed Mach number a flutter boundary usually is characterized by only a slight variation of dynamic pressure over a substantial range of density. Furthermore, such flutter boundaries are often also characterized by a nearly constant flutter frequency  $\omega$ . Thus, where both of these characteristics are present,  $\rho$  is closely proportional to  $k^2$ .

Study of equation (A12) indicates that flutter boundaries can be expressed in terms of four nondimensional quantities as follows: Mach number  $M$ , reduced frequency  $k$ , mass ratio  $\mu$ , and frequency ratio  $\omega/\omega_B$ , and by combinations of the four. (Mass ratio  $\mu$  is the ratio of wing mass to the mass of air in a cone or truncated cone that encloses the wing.) For example, by combining either

$$\frac{\omega}{\omega_B} \frac{1}{k} = \frac{V}{b_0 \omega_B} \quad (\text{A16a})$$

$$Mk\sqrt{\mu} \frac{\omega_B}{\omega} = \frac{b_0 \omega_B}{a} \sqrt{\mu} \quad (\text{A16b})$$

or

$$k\sqrt{\mu} \frac{\omega_B}{\omega} = \frac{b_0 \omega_B}{V} \sqrt{\mu} \quad (\text{A16c})$$

the results are measures of stiffnesses required in terms of  $b_0 \omega_B$  to prevent flutter for a given  $M$  or  $V$ , and  $\rho$  (contained in  $\mu$ ). The first combination (eq. (A16a)) has been termed a flutter index or flutter-speed ratio. The second combination (eq. (A16b)) has been called a stiffness-altitude parameter. (See, for example, ref. 2.) The third combination (eq. (A16c)) is a variation of the second, differing only by the Mach number.

In comparing calculated and experimental results, commonly only two of the four quantities  $M$ ,  $k$ ,  $\mu$ , and  $\omega/\omega_B$  can be matched. In the present study,  $M$  and  $\mu$  were matched. Differences between calculated and experimental flutter index or stiffness-altitude parameters are interpreted as indicating that the wing stiffness in terms of  $b_0 \omega_B$  from the analysis is greater or less than required to match the experimental counterparts. Differences in flutter-frequency ratio also usually occur. The magnitudes and trends of these two differences are measures of the adequacy of the analysis as applied to the experiments in the present study.

In the discussion following equation (A15), the usual trend of eigensolution results was described. Occasionally, however, one or more eigenvalues  $\Omega$  will indicate an instability (a positive  $g$ ) for low  $\rho$  and low  $k$ . (Note that the minus sign must be included with the downwash ratio on the left-hand side of eq. (6). The wrong sign here can make all modes appear to be unstable, rather than stable.) A flutter instability for

## APPENDIX A – Concluded

low  $k$  and low  $\rho$  usually means an essentially single-degree-of-freedom flutter. This type of instability is revealed by a positive sign of the imaginary part of  $Q_{ii}$ , where mode  $i$  is the predominant modal element in the flutter eigenvector. Single-degree flutter boundaries are usually strongly dependent on how much structural damping is present. Furthermore, the associated value of  $\rho$  may be so low as to be above the altitude range of interest, and when  $k$  is increased to extend the flutter boundary to higher  $\rho$  (lower altitude), the imaginary part of  $Q_{ii}$  may become negative (stable), and only the more usual coupled-mode flutter is then possible.

In appendix B, an example of a flutter calculation is carried through.

## APPENDIX B

### A COMPUTED FLUTTER EXAMPLE

To illustrate the calculation of a flutter boundary, the 70° swept delta-wing model (model 1A of ref. 2) was chosen largely because some comparisons of approximate downwash distributions with the called for downwash at 46 downwash control points are already available in figure 5 of reference 1.

The first major step in computing the flutter boundary for a given wing is to choose the parameters  $M$  and  $k$  and to choose the locations of the array of downwash control points. In order to solve matrix equation (32) of reference 1 for the weighting factors  $a_{nm}^{(j)}$ , the downwash quantities  $-\partial h_j / \partial x$  and  $-2h_j$  must be supplied for each control point and each mode. (In the program the imaginary part of the downwash is multiplied by  $k$ .)

#### Location of Control Points and Determination of Downwash

Since four modes were used in this example, it was desired to take advantage of the full program capacity of 48 downwash control points rather than the 46 with which the results of reference 1 were obtained. These 48 points were distributed as follows: for even tenths of the semispan, points were located at 20, 40, 60, 80, and 100 percent of the local chord; for odd tenths, points were located at 10, 30, 50, 70, and 90 percent of the local chord; except that at 0.9 semispan no point at 10-percent chord was used, at 0.1 semispan no points at 30- or 70-percent chord were used, and at the plane of symmetry a point was located at 3 percent of the local chord.

Values of measured modal deflections are listed in table II of reference 2 for each tenth of the semispan at the 0.0, 0.25, 0.50, 0.75, and 1.00 local-chord locations for four modes. The semispan location of the control points of the present analysis correspond to the measurement points of the model of reference 2; however, the chord locations do not correspond. It is, therefore, necessary to use some chordwise interpolation scheme to provide values of deflections and of deflection slopes. A polynomial approximation in powers of the chordwise coordinate was used for this interpolation; the second and third chordwise derivatives were made zero as approximations for zero conditions of bending moment and shear at leading and trailing edges; that is, to use for each span station and each mode

$$\left. \begin{aligned} h(\bar{x}) &= d_0 + d_1 \bar{x} + d_2 \bar{x}^2 + \dots + d_8 \bar{x}^8 \\ \text{and} \quad \frac{\partial^2 h(0)}{\partial \bar{x}^2} &= \frac{\partial^3 h(0)}{\partial \bar{x}^3} = \frac{\partial^2 h(1)}{\partial \bar{x}^2} = \frac{\partial^3 h(1)}{\partial \bar{x}^3} = 0 \end{aligned} \right\} \quad (B1)$$

APPENDIX B - Continued

where  $\bar{x}$  is the local chordwise coordinate with values 0 and 1 at leading and trailing edges, respectively. The local chordwise coordinate is

$$\bar{x} = \frac{x - x_{1e}}{x_{te} - x_{1e}} \quad (B2)$$

The leading-edge conditions cause

$$a_2 = a_3 = 0$$

and equations (B1) become

$$\left. \begin{aligned} h(\bar{x}) &= d_0 + d_1\bar{x} + d_4\bar{x}^4 + d_5\bar{x}^5 + \dots + d_8\bar{x}^8 \\ \text{and} \\ \frac{\partial^2 h(1)}{\partial \bar{x}^2} &= \frac{\partial^3 h(1)}{\partial \bar{x}^3} = 0 \end{aligned} \right\} \quad (B3)$$

Solutions for the seven unknown coefficients  $d_r$  are made from seven simultaneous equations obtained by applying the five deflections and the two trailing-edge conditions. The slope  $\partial h_j / \partial x$  needed in the real part of the downwash is

$$\frac{\partial h_j}{\partial x} = \frac{\partial h(\bar{x})}{\partial \bar{x}} \frac{\partial \bar{x}}{\partial x} = \frac{1}{(x_{te} - x_{1e})} (d_1 + 4d_4\bar{x}^3 + 5d_5\bar{x}^4 + 6d_6\bar{x}^5 + 7d_7\bar{x}^6 + 8d_8\bar{x}^7) \quad (B4)$$

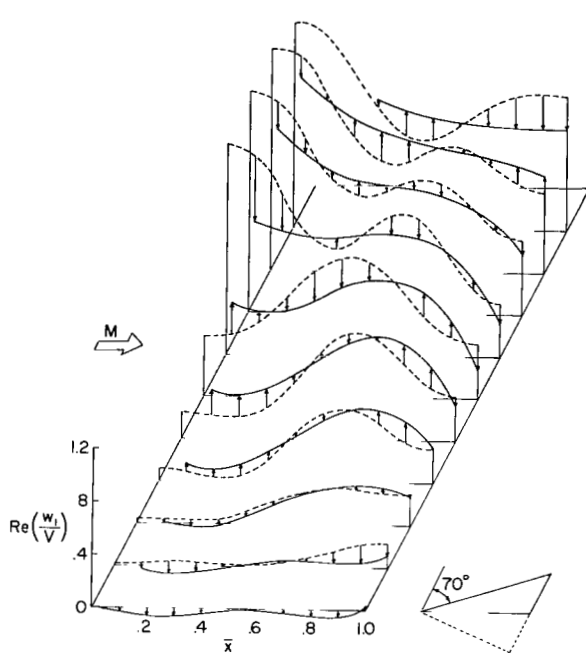
Some results of this type of interpolation are presented in the following section.

Solution for Weighting Factors  $a_{n,m}^{(j)}$

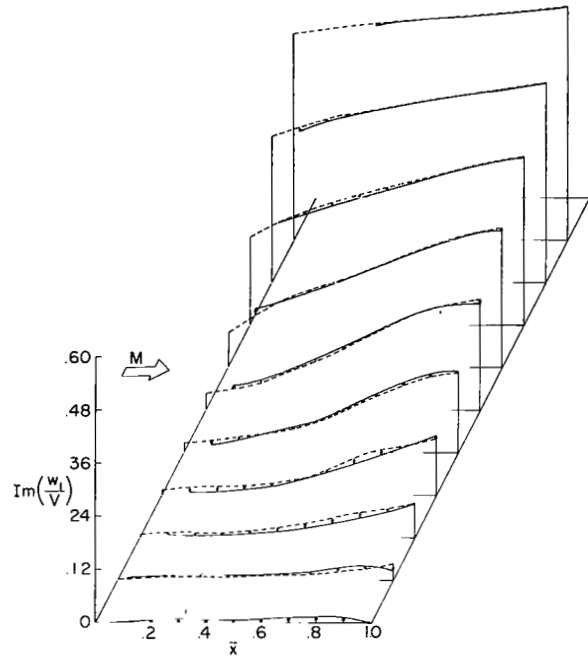
Values for the downwash quantities  $-\partial h_j / \partial x$  and  $-2h_j$  for each collocation point and each mode are supplied along with the other necessary input data. Equation (32) of reference 1 is solved for the column of  $a_{n,m}^{(j)}$  for each mode  $j$  by a least-square-error subroutine. Also produced during this type of solution is a matrix of residuals that are of interest; these are the differences between the called for downwash and the least-square solution at the control points. Solutions for the  $a_{n,m}^{(j)}$  actually determine distributions over the wing of both lifting pressure and associated downwash. Additional values of the downwash at other points on the wing can be obtained by supplying the input data for those points, computing the matrix  $\Pi_{nm}$  of equation (28) of reference 1, and then carrying out the multiplication on the right-hand side of equation (32) of reference 1.

Results from such a sequence of operations are shown in figure 8 for four modes of the example flutter model. In order to display the results more clearly, the delta semi-span planform is transformed to a rectangle. The short-dash lines indicate the desired downwash distribution determined by means of the interpolation process described in this appendix. The real and imaginary parts come from equations (B4) and (B3), respectively.

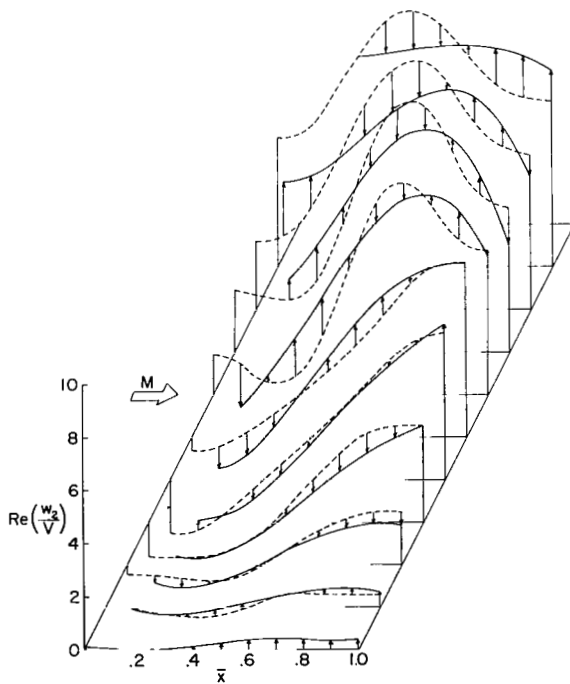
APPENDIX B - Continued



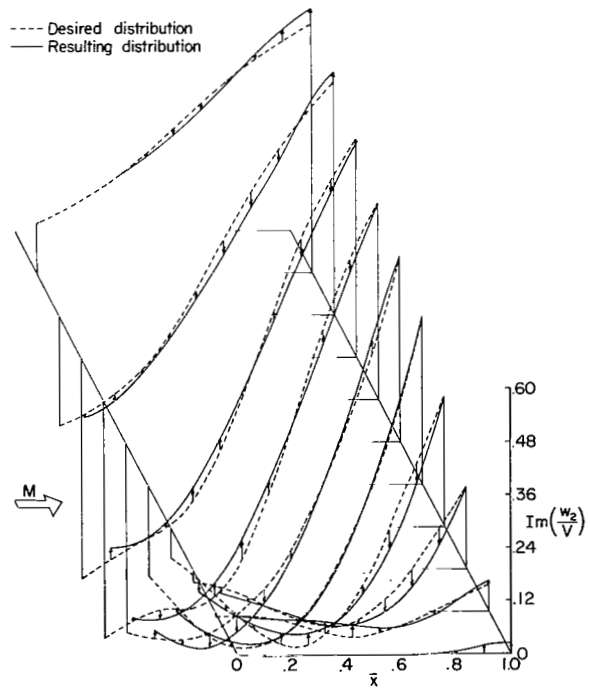
(a) Real part, mode 1.



(b) Imaginary part, mode 1.



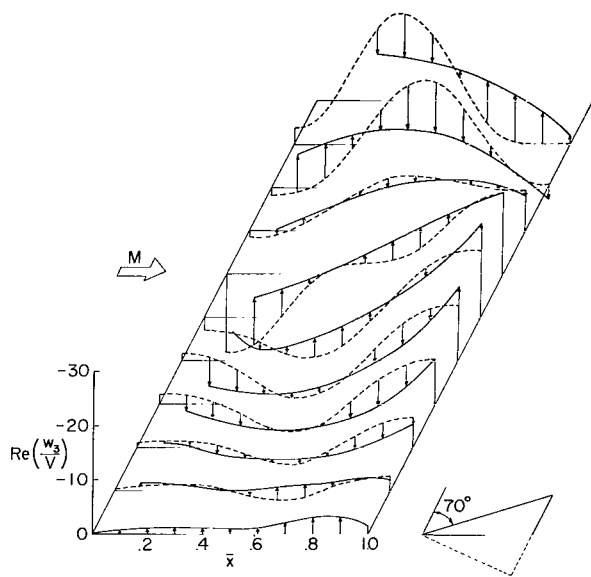
(c) Real part, mode 2.



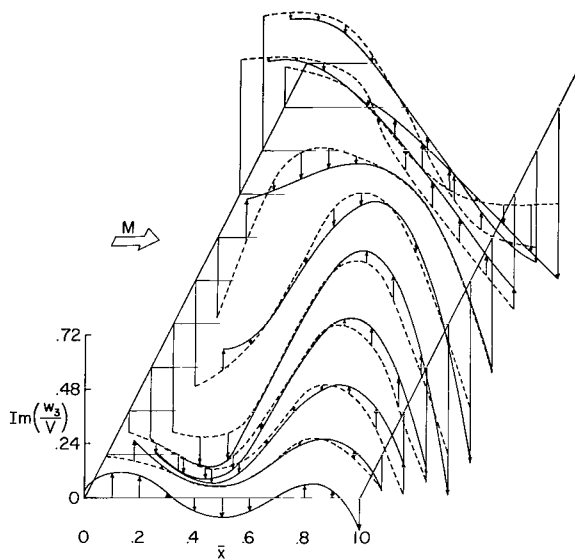
(d) Imaginary part, mode 2.

Figure 8.- Downwash distributions over right semispan for the four modes used in the flutter example for model 1A.

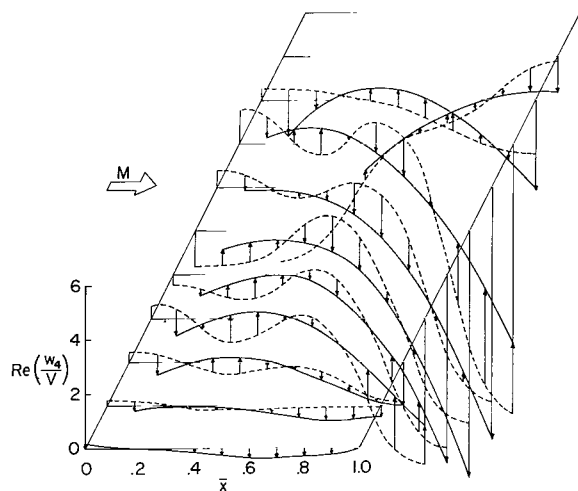
APPENDIX B - Continued



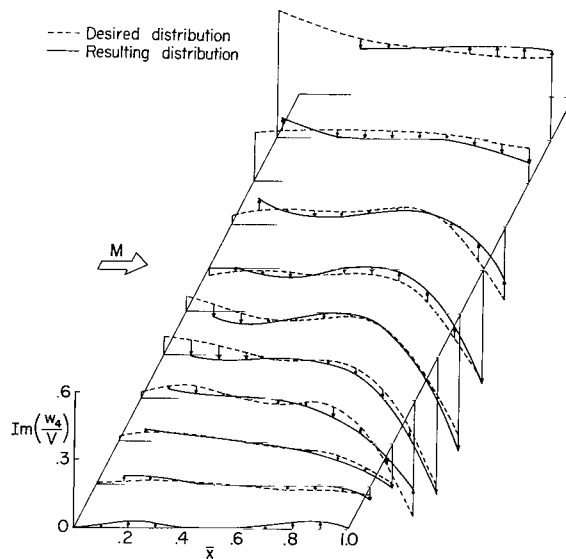
(e) Real part, mode 3.



(f) Imaginary part, mode 3.



(g) Real part, mode 4.



(h) Imaginary part, mode 4.

Figure 8.- Concluded.

## APPENDIX B - Continued

The solid lines indicate the least-square solution obtained by the collocation procedure. The quality of the comparison of the two is readily observed. The agreement was good for the smoother downwashes; however, for the downwash distributions that fluctuated rather abruptly, particularly those for the real parts of the modes, the approximate downwashes did not follow the prescribed variations in detail.

### Generalized Aerodynamic Forces

The nondimensional generalized aerodynamic-force elements  $Q_{ij}^*$  are calculated according to the "standard" choice; that is, chordwise integration by a 10-point Gaussian rule and spanwise integration by Simpson's rule. The modal deflections  $h_i$  are supplied as input data for each tenth of the local chord at each tenth of the semispan; these deflections were computed according to equations (B3) on the basis of the mode-shape data from table II(a) of reference 2. To compute the deflections  $h_i(x_c)$  at the chordwise-integration points, a subroutine performs a second-order (parabolic) interpolation from the input data. (The subroutine can do a first order (linear) interpolation as an option.)

### Solution of the Flutter Determinant

In addition to the generalized aerodynamic forces, the input data needed for use in calculating the flutter-determinant elements are the generalized masses, the modal frequencies and a base frequency, the modal damping coefficients, and a sequence of values of the air-mass parameter  $\alpha$ . The cyclic frequencies  $f_2$  and air density in  $\alpha$  are obtained from table I of reference 2 for model 1A at  $M = 2.0$ . The frequency  $\omega_2$  ( $\omega_2 = 2\pi f_2$ ) is used as  $\omega_B$ , and damping coefficients  $g_{i,S} = 0$  are used. The same generalized masses as those for the piston-theory analysis are used:

$m_{11} = 0.0001905 \text{ slug} \cdot \overset{0.002780}{(0.0002583 \text{ kg})}$ ,  $m_{22} = 0.0003801 \text{ slug} \cdot \overset{0.005547}{(0.0005153 \text{ kg})}$ ,  
 $m_{33} = 0.0004918 \text{ slug} \cdot \overset{0.007177}{(0.0006667 \text{ kg})}$ ,  $m_{44} = 0.0001271 \text{ slug} \cdot \overset{0.001855}{(0.0001723 \text{ kg})}$ ,  
 other  $m_{ij} = 0$ . A sequence of air densities that extend from well below to well above the experimental value are used in  $\alpha$ . The reduced frequency  $k$  of the experiment was 0.283, so a nearby value of  $k = 0.3$  is used initially in the analysis. (A point to be noted is that reference 2 uses for semichord the value at the 75-percent semispan station ( $b_{.75s}$ ), while the present report uses the value at the root ( $b_0$ ).)

As described in appendix A, for each value of  $\alpha$  a flutter determinant is formed and the eigenvalues  $\Omega$  are computed. From each  $\Omega$ , a damping coefficient  $g$ , a frequency ratio  $\omega_B/\omega$ , and frequency  $\omega$  are obtained, and the product  $(\omega_B/\omega)k$  is a stiffness parameter  $\frac{b_0\omega_B}{V} = \frac{b_0\omega_2}{V}$  since  $\omega_2$  was chosen as  $\omega_B$ .

Figure 9 shows the damping coefficients  $g$ , and the stiffness parameter  $b_0\omega_2/V$  as functions of the air-mass parameter  $\alpha$ . All four of the  $g$  curves depart from the

APPENDIX B - Continued

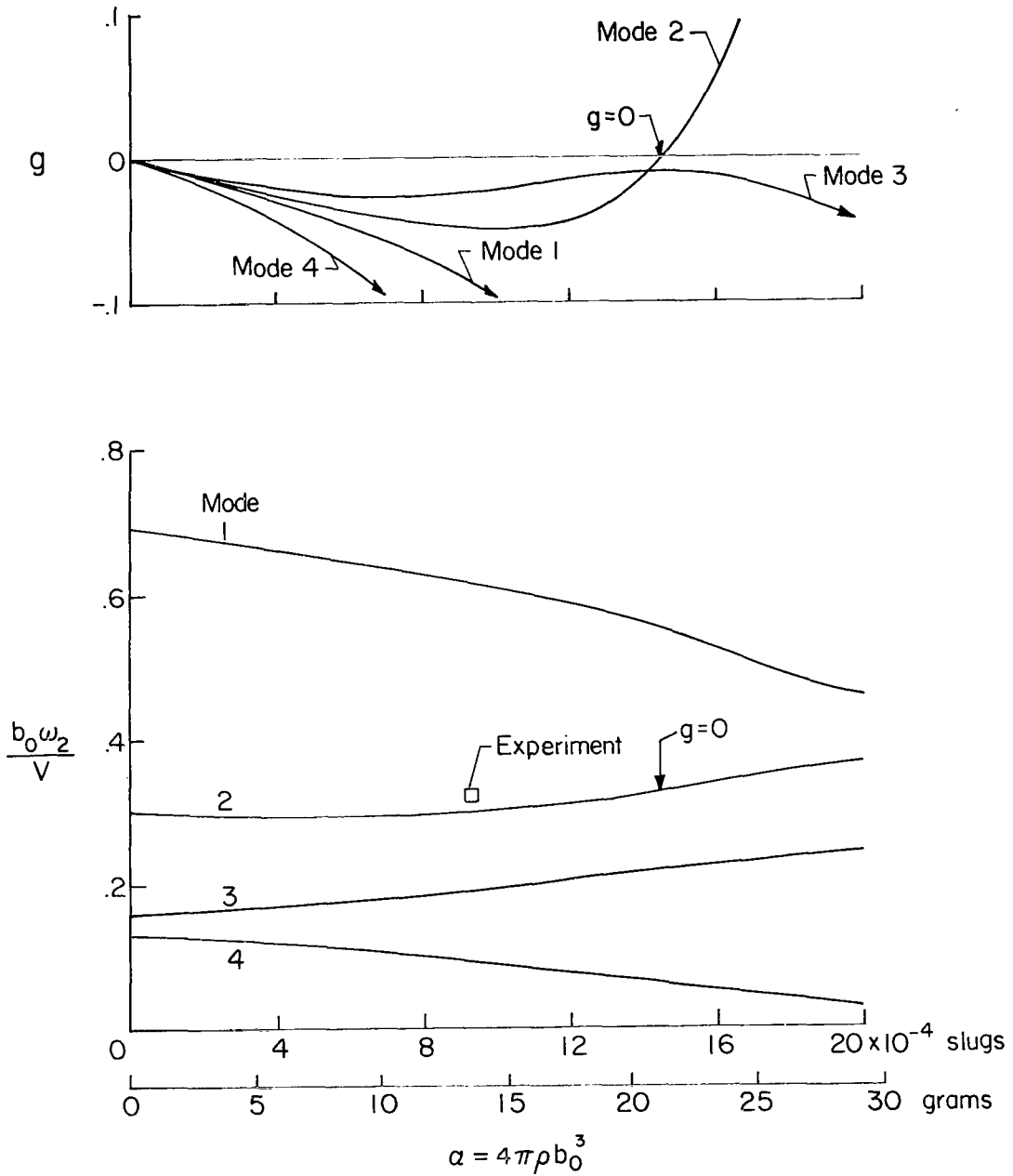


Figure 9.- Structural damping coefficient  $g$  and stiffness parameter  $b_0 \omega_2 / V$  as a function of air-mass parameter  $\alpha$  for the flutter example.  $M = 2$ ;  $k = 0.3$ .

APPENDIX B - Continued

origin into the negative region, thus dynamic stability is indicated. As the air density  $\rho$  is increased sufficiently, the mode 2 curve passes upward through  $g = 0$  and indicates the value of  $\alpha$  for which the mode 2 curve of the stiffness parameter penetrates into a flutter region.

For the value of  $k$  used in this example (0.3), the value of  $\alpha$  is considerably higher than that of the experiment, which indicates that lower values of  $k$  should be used. Two additional values of  $k$  (0.22 and 0.25) were used to enable the plotting of a flutter boundary through the experimental value of the air-density parameter. The analytical and experimental results are presented in the following table and in figure 10.

	$k$	$\frac{\rho}{\rho_{exp}}$	$\frac{b_0 \omega_2}{V}$	$\frac{b .75 s \omega_2}{a} \sqrt{\mu}$	$\frac{\omega}{\omega_2}$	$\frac{\omega_{th}}{\omega_{exp}}$
Analysis	0.22	0.85	0.239	0.860	0.921	1.04
	.25	1.08	.275	.862	.919	1.04
	.30	1.57	.324	.855	.926	1.05
Experiment	0.283	1.00	0.320	1.06	0.885	1.00

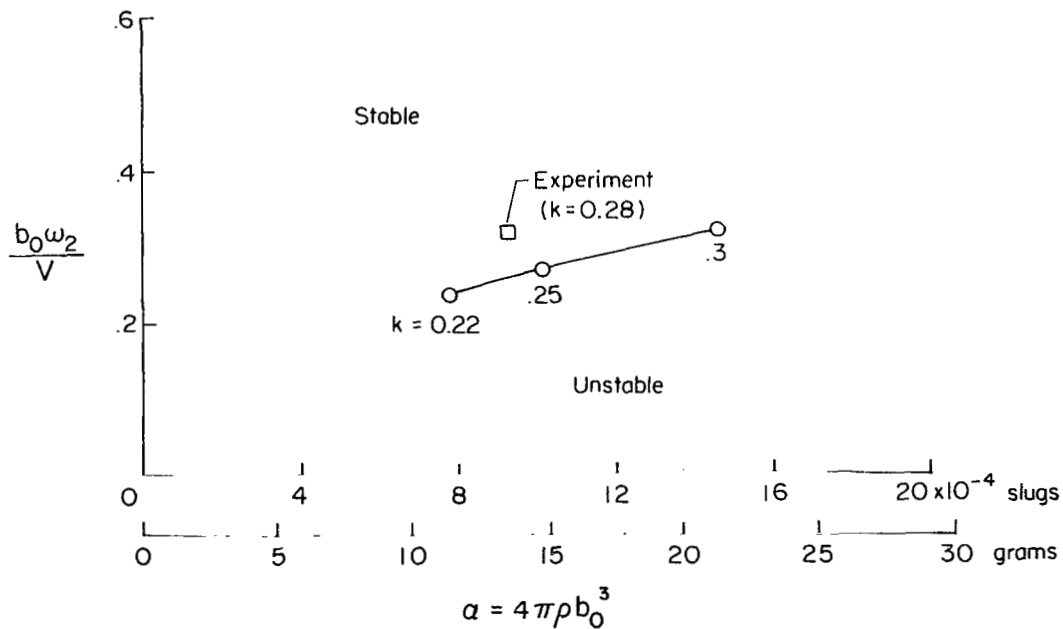


Figure 10.- Analytical flutter-boundary segment for the flutter example.  
 $M = 2$ ;  $g = 0$ .

APPENDIX B - Continued

A feature to be noted from the analytical results presented in the previous table is that over the 85-percent variation of the air-density parameter (column 2), the stiffness-altitude parameter (column 4), and the frequency ratio (column 5) vary by less than 1 percent. In comparison with experimental results, the analytical results are unconservative; that is, they predict this model to flutter when the stiffness-altitude parameter is less than about 0.86, whereas the experimental results indicate flutter for a stiffness-altitude parameter less than 1.06.

In searching for reasons why the analytical result is so unconservative, it was decided to recompute the generalized masses  $m_{ij}$  and, thus, make use of the mode shapes interpolated from equation (B3). The numerical surface integrations produced the following matrix in units of ~~slug-ft<sup>2</sup> (kg-m<sup>2</sup>)~~  $\text{slugs (kg)}$  that can be compared with the values cited previously in the text:

$$[m_{ij}] = 10^{-6} \begin{bmatrix} 182 & -0.4 & 17.2 & 8.6 \\ \cancel{(247)} & \cancel{(-0.5)} & \cancel{(23.3)} & \cancel{(11.7)} \\ (2656) & (-6) & (251) & (126) \\ & 356 & -89.2 & -29.8 \\ & \cancel{(483)} & \cancel{(-120.9)} & \cancel{(-40.4)} \\ & (5195) & (-1302) & (-435) \\ & & 472 & 41.0 \\ & & \cancel{(640)} & \cancel{(-55.6)} \\ & & (6888) & (598) \\ \text{Symmetric} & & & 128 \\ & & & \cancel{(174)} \\ & & & (1868) \end{bmatrix}$$

For  $k = 0.25$  the results are

k	$\frac{\rho}{\rho_{\text{exp}}}$	$\frac{b_0 \omega_2}{V}$	$\frac{b .75s \omega_2 \sqrt{\mu}}{a}$	$\frac{\omega}{\omega_2}$	$\frac{\omega_{\text{th}}}{\omega_{\text{exp}}}$
0.25	1.05	0.272	0.890	0.920	1.04

In comparison to the previous table, the value of the stiffness-altitude parameter is increased by only about 3 percent toward the experimental value and is still unconservative. A natural speculation is then to attribute the remaining unconservativeness either to the analytical aerodynamics or to some unknown and unaccounted for characteristic of the experimental model, such as internal stresses due to thermal gradients. Thermal gradients were known to be present in the vicinity of the root, which had been tightly clamped along its full chord while at room temperature, but quantitative information is lacking. Another speculative possibility, though a minor one, is that the mode shapes of

## APPENDIX B - Concluded

the models actually flutter tested were a little different from the "representative mode shapes" used here from table II(a) of reference 2. No study has been made of the sensitivity of the analytical-flutter results to variations in mode shape. Such a study would have a great number of independent variables and is beyond the scope of the present report.

## REFERENCES

1. Cunningham, Herbert J.: Improved Numerical Procedure for Harmonically Deforming Lifting Surfaces From the Supersonic Kernel Function Method. AIAA J., vol. 4, no. 11, Nov. 1966, pp. 1961-1968.
2. Hanson, Perry W.; and Levey, Gilbert M.: Experimental and Calculated Results of a Flutter Investigation of Some Very Low Aspect-Ratio Flat-Plate Surfaces at Mach Numbers From 0.62 to 3.00. NASA TN D-2038, 1963.
3. Cunningham, Herbert J.; and Woolston, Donald S.: Developments in the Flutter Analysis of General Plan Form Wings Using Unsteady Air Forces From the Kernel Function Procedure. Proc. Nat. Specialists Meeting on Dynamics and Aeroelasticity (Fort Worth, Texas), Inst. Aero. Sci., Nov. 1958, pp. 27-36.
4. Hanson, Perry W.: Experimental Determined Effects of Varying Pitch and Control Stiffnesses on the Flutter Characteristics at Supersonic Speeds of All-Movable Wing and Tail Models. NASA MEMO 10-16-58L, 1959.
5. Curtis, Alan R.; and Lingard, Robert W., Jr.: Unsteady Aerodynamic Distributions for Harmonically Deforming Wings in Supersonic Flow. AIAA Pap. No. 68-74, Jan. 1968.
6. Bisplinghoff, Raymond L.; and Ashley, Holt: Principles of Aeroelasticity. John Wiley & Sons, Inc., c.1962, pp. 404-408.
7. Cunningham, Herbert J.: Flutter Analysis of Flat Rectangular Panels Based on Three-Dimensional Supersonic Unsteady Potential Flow. NASA TR R-256, 1967.
8. Francis, J. G. F.: The QR Transformation - A Unitary Analogue to the LR Transformation. Comput. J., vol. 4.  
Part 1 - Oct. 1961, pp. 265-271.  
Part 2 - Jan. 1962, pp. 332-345.

TABLE I.- FLUTTER RESULTS FOR MODELS 1A AND 1C

M	$\frac{b.75s\omega_2}{a}\sqrt{\mu}$		$\frac{\omega_{th}}{\omega_{exp}}$	k	
	Experiment (ref. 2)	Present analysis		Experiment (ref. 2)	Present analysis
Model 1A					
1.19	0.82	0.780	0.988	0.347	0.325
1.30	.78	.782	.890	.371	.330
1.64	.88	.820	.946	.335	.294
2.00	1.06	.891	1.024	.283	.244
2.55	1.11	1.002	1.018	.256	.234
2.90	---	1.090	} 1.008	{ ----	.237
3.00	1.12	----			.234
Model 1C					
1.16	0.90	0.800	1.072	0.812	0.78
1.30	.91	.878	.952	.855	.79
1.64	1.09	1.01	.966	.743	.67
2.00	1.31	1.21	1.035	.572	.55
3.00	2.00	1.51	1.197	.420	.378

TABLE II.- MODE-SHAPE AND OTHER DATA FOR MODEL HT-7\*

Chord, percent	Normalized deflection at semispan locations (in percent) of -										
	0	10	20	30	40	50	60	70	80	90	100
$\omega_1 = 2\pi(162.5)$ ; $m_{11} = 0.000357$ slug <sup>0.000357</sup> ( <del>0.000484</del> kg)											
0	-0.218	-0.192	-0.158	-0.110	-0.047	0.036	0.137	0.252	0.385	0.525	0.675
25	-.148	-.106	-.058	.013	.060	.140	.237	.345	.468	.607	.752
50	-.027	.009	.044	.093	.155	.233	.326	.434	.557	.686	.825
75	.047	.095	.145	.200	.262	.335	.426	.527	.644	.765	.907
100	.188	.230	.271	.320	.376	.442	.525	.621	.735	.860	1.000
$\omega_2 = 2\pi(391)$ ; $m_{22} = 0.000518$ slug <sup>0.000518</sup> ( <del>0.000702</del> kg)											
0	1.000	0.721	0.545	0.455	0.388	0.350	0.328	0.328	0.385	0.504	0.639
25	.549	.408	.307	.271	.259	.257	.255	.266	.336	.466	.598
50	.138	.131	.136	.149	.165	.182	.202	.234	.309	.436	.558
75	-.156	-.215	-.257	-.278	-.271	-.223	-.073	.175	.300	.415	.512
100	-.466	-.482	-.487	-.468	-.418	-.351	-.271	.058	.284	.400	.497
$\omega_3 = 2\pi(725)$ ; $m_{33} = 0.000264$ slug <sup>0.000264</sup> ( <del>0.000358</del> kg)											
0	0.122	0.035	-0.053	-0.166	-0.335	-0.454	-0.505	-0.498	-0.375	0.075	0.534
25	.026	-.044	-.122	-.221	-.316	-.368	-.371	-.317	-.171	.258	.659
50	-.084	-.132	-.179	-.236	-.284	-.297	-.274	-.195	.080	.474	.757
75	-.115	-.153	-.196	-.232	-.249	-.241	-.154	.118	.395	.629	.868
100	-.140	-.180	-.213	-.232	-.219	-.126	.124	.388	.600	.798	1.000

\*Mass of model, 0.00528 slug (0.0770 kg).

NATIONAL AERONAUTICS AND SPACE ADMINISTRATION  
WASHINGTON, D. C. 20546  
OFFICIAL BUSINESS

FIRST CLASS MAIL



POSTAGE AND FEES PAID  
NATIONAL AERONAUTICS AND  
SPACE ADMINISTRATION

17U 001 26 51 3DS 70316 00903  
AIR FORCE WEAPONS LABORATORY /WLOL/  
KIRTLAND AFB, NEW MEXICO 87117

ATT E. LOU BOWMAN, CHIEF, TECH. LIBRARY

POSTMASTER: If Undeliverable (Section 158  
Postal Manual) Do Not Return

*"The aeronautical and space activities of the United States shall be conducted so as to contribute . . . to the expansion of human knowledge of phenomena in the atmosphere and space. The Administration shall provide for the widest practicable and appropriate dissemination of information concerning its activities and the results thereof."*

— NATIONAL AERONAUTICS AND SPACE ACT OF 1958

## NASA SCIENTIFIC AND TECHNICAL PUBLICATIONS

**TECHNICAL REPORTS:** Scientific and technical information considered important, complete, and a lasting contribution to existing knowledge.

**TECHNICAL NOTES:** Information less broad in scope but nevertheless of importance as a contribution to existing knowledge.

**TECHNICAL MEMORANDUMS:** Information receiving limited distribution because of preliminary data, security classification, or other reasons.

**CONTRACTOR REPORTS:** Scientific and technical information generated under a NASA contract or grant and considered an important contribution to existing knowledge.

**TECHNICAL TRANSLATIONS:** Information published in a foreign language considered to merit NASA distribution in English.

**SPECIAL PUBLICATIONS:** Information derived from or of value to NASA activities. Publications include conference proceedings, monographs, data compilations, handbooks, sourcebooks, and special bibliographies.

**TECHNOLOGY UTILIZATION PUBLICATIONS:** Information on technology used by NASA that may be of particular interest in commercial and other non-aerospace applications. Publications include Tech Briefs, Technology Utilization Reports and Notes, and Technology Surveys.

*Details on the availability of these publications may be obtained from:*

SCIENTIFIC AND TECHNICAL INFORMATION DIVISION  
NATIONAL AERONAUTICS AND SPACE ADMINISTRATION  
Washington, D.C. 20546